IEIE Transactions on Smart Processing and Computing, vol. 3, no. 4, August 2014
http://dx.doi.org/10.5573/IEIESPC.2014.3.4.212

Development of Millimeter-Wave Communication Modem for Mobile Wireless Backhaul in Mobile Hotspot Network

Seung Nam Choi[1], Junhyeong Kim[1], Il Gyu Kim[1], and Dae Jin Kim[2]

[1] Wireless Transmission Research Department, Electronics and Telecommunications Research Institute / 218 Gajeong-ro, Yuseong-gu, Daejeon, 305-700, KOREA {choisn, jhkim41jf, igkim}@etri.re.kr
[2] School of Electronics and Computer Engineering, Chonnam National University / 77 Yongbong-ro, Buk-gu, Gwangju, 500-757, KOREA djinkim@chonnam.ac.kr

***** Corresponding Author: Dae Jin Kim

Received December 20, 2013; Revised February 27, 2013; Accepted May 12, 2014; Published August 31, 2014

** Regular Paper*

** Extended from a Conference: Preliminary results of this paper were presented at the IEEE ISCE 2014. This present paper has been accepted by the editorial board through the regular reviewing process that confirms the original contribution.*

***Abstract*:** The current cellular communications are optimized for low mobility users, meaning that their performance is degraded at high speed. Therefore, passengers in a high-speed train experience very poor radio link quality due to the significantly large number of simultaneous handovers. In addition, wireless data traffic is expanding exponentially in trains, subways and buses due to the widespread use of smartphones and mobile devices. To solve the inherent problem of cellular communication networks and meet the growing traffic demand, this paper proposes the mobile hotspot network of a millimeter-wave communication system as a mobile wireless backhaul. This paper describes the physical layer design of uplink and downlink in the proposed system, and the performances of uplink and downlink are evaluated under Rician fading channel conditions. The implemented baseband prototype of the proposed millimeter-wave communication modem is presented. This system can provide a Gbps data rate service in high-speed trains carrying hundreds of wireless Internet users.

***Keywords*:** Millimeter-wave, Wireless backhaul, Mobile hotspot network, Distributed antenna system

1. Introduction

The widespread use of smartphones and mobile devices has created a strong demand for high data rate services in trains, subways, and buses carrying hundreds of Internet users. Despite this, current cellular communication networks, such as LTE/LTE-Advanced have been optimized for low mobility users and their performance is degraded at high speed. Therefore, passengers in a high-speed train (350 km/h) experience very poor multimedia services and discontinuous connections due mainly to the insufficient bandwidth and much more frequent handover failures.

Research on the seamless wireless connectivity of LTE networks in high-speed trains (350 km/h) was performed because the large number of frequent handovers across cells greatly increases the possibility of service interruptions [1]. In Taiwan, the integrated Worldwide Interoperability for Microwave Access-Radio over Fiber (WiMAX-RoF) architecture was proposed and tested to achieve a high data rate (10 Mbps) at high mobility (300 km/h), which is a type of mobile backhaul system [2]. In the ITU-R IMT-Advanced requirements, the peak useful data rate is 1000 Mbps in a pedestrian speed, which decreases to 100 Mbps at speeds beyond 250 km/h [3]. The peak data rates in the LTE-Advanced system are 1000 Mbps in the downlink and 500 Mbps in the uplink [4]. On the other hand, to prepare for future mobile data growth, the 3GPP (3rd Generation Partnership Project) began to examine the small cell technology as one approach that can achieve up to 1000 times higher capacity than currently available [5]. The three topics are improvements in spectral efficiency, additional spectrum and large number of small base stations. The spectrum for small cells is below 6 GHz or above 6 GHz including the millimeter band region. But small cells are still appropriate for low

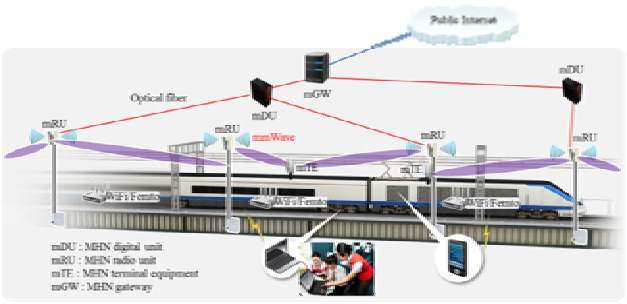

Fig. 1. Mobile hotspot network structure based on millimeter-wave communications for high-speed trains.

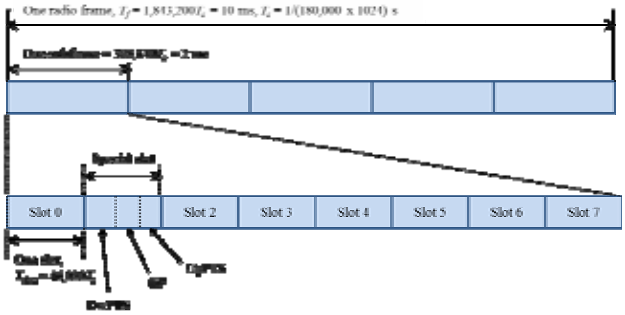

Fig. 2. TDD frame structure.

mobility users.

New communication systems are urgently required to handle group mobility patterns and the exponential increased traffic in wireless environments, such as trains, subways and buses. Therefore, a distributed antenna system (DAS) based on a millimeter-wave mobile broadband communication system for a high-speed train (HST) was introduced [6, 7]. This type of system is called a mobile hotspot network (MHN).

This paper proposes the physical layer design of uplink and downlink in a MHN acting as a mobile wireless backhaul. The performance of the uplink and downlink were evaluated under Rician fading channel, which is assumed in a HST scenario, and the implemented baseband prototype of the proposed millimeter-wave communication modem is presented.

2. Mobile Hotspot Network

Fig. 1 shows the MHN structure based on millimeter-wave (mmWave) communications for HSTs. The structure consists of digital units (mDUs) with multiple radio units (mRUs), terminal equipments (mTEs) and gateways (mGWs). Each mDU, which is interconnected with multiple mRUs via optical fibers, is responsible for baseband signal processing. This system introduces the DAS concept that mRUs are deployed along the railway. The distance between the adjacent mRUs should be much smaller than the distance between the base stations of the existing cellular systems to overcome the coverage problems due to the propagation characteristics of millimeter-wave communications. In addition, both mDUs and mTEs use Tx/Rx beamforming (BF) for the coverage improvement. The BF enhances the desired signal strength while suppressing the interference signals from the other mRUs. The 27 GHz band was used to provide a mobile wireless backhaul for HST. The millimeter-wave backhaul signals are converted to WiFi/Femto signals inside the train.

Each mRU functions as a base station and has a unique cell identity. The BF makes it possible to maintain multiple independent radio links between the mRUs and mTEs. As a result, different data streams can be transmitted /received to/from mRUs. Multiple antennas of mTE are installed to reduce the handover latency by maintaining the multiple connections to mRUs. Each antenna on the train, which is interconnected with its corresponding modem in the mTE, switches the serving mRU independently and the probability of losing all the links at the same time is almost zero, which minimizes the link failure rate during handover. In addition, this structure enables mRUs to use the same radio resource simultaneously, which improves the spectrum efficiency significantly.

3. mmWave Communication System

This section describes the MHN frame structure and the physical layer design of the uplink and downlink.

3.1 Frame Structure

In a MHN, the downlink and uplink transmissions are organized into radio frames with a $T_f = 1843200 \times T_s = 10$ ms duration. The basic time unit, T_s, is 1/(180000×1024) second. Time division duplexing (TDD) and frequency division duplexing (FDD) radio frame structures are supported, but only the TDD is described in this paper.

Owing to the enormous spectrum available in the millimeter-wave, carrier aggregation can be used in the system to increase the system bandwidth. Each aggregated carrier is generally referred to as a component carrier. The transmissions in multiple component carriers can be aggregated where up to three secondary component carriers can be used in addition to the primary component carrier. In the case of carrier aggregation, the mTE may assume that the same frame structure is used in all the serving component carriers. One component carrier has 125 MHz and four component carriers occupy a 500 MHz bandwidth.

In the TDD frame structure of Fig. 2, each radio frame with length, $T_f = 1843200 \cdot T_s = 10$ ms, consists of five subframes with lengths, $368640 \cdot T_s = 2$ ms each. Each subframe consists of eight slots with lengths, $46080 \cdot T_s = 250$ μs. Fig. 3 shows the supported uplink-downlink configurations, where “D” denotes the slot reserved for downlink transmissions, “U” denotes the slot reserved for uplink transmissions and “S” denotes a special slot with three fields, DwPTS (downlink pilot timeslot), GP (guard period) and UpPTS (uplink pilot timeslot). Table 1 lists the

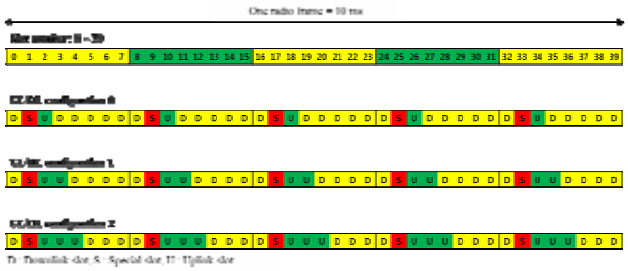

Fig. 3. Uplink-downlink configurations.

Table 1. Configuration of the special slot (lengths of DwPTS/GP/UpPTS).

Special slot configuration	DwPTS	UpPTS
0	**39168·T_s**	**4608·T_s**
1	36864·T_s	
2	34560·T_s	

length of DwPTS and UpPTS subject to the total length of the DwPTS, GP and UpPTS being equal to 46080·T_s = 250 μs. These configurations are the same in every subframe.

The uplink-downlink configurations with a 2 ms downlink-to-uplink switch-point periodicity are supported. In this case, the special slot exists in the second slot of each subframe. In addition, the first slot of each subframe is always reserved for downlink transmission. UpPTS and the slot immediately following the special slot are always reserved for uplink transmission. When multiple component carriers are aggregated, the mTE may assume the same uplink-downlink configuration and the same special slot configuration across all the component carriers.

This system defines the slot as a transmission time interval (TTI), which means scheduling occurs every 250 μs. One slot consists of 40 orthogonal frequency division multiplexing (OFDM) symbols, each 6.25 μs in length, as shown in Fig. 4. Table 2 lists the system parameters related to OFDM numerology, where the values are decided carefully considering the millimeter-wave channel properties. The system bandwidth of a component carrier is 125 MHz corresponding to 50 resource blocks. Each resource block consists of twelve subcarriers where the subcarrier spacing is 180 kHz. The sampling rate is equal to 1/T_s = 184.32 MHz, indicating that a high-speed modem design is very important. An OFDM symbol length (FFT size) is 1024 samples and the cyclic prefix (CP) length is 128 samples, respectively.

3.2 Uplink

The uplink transmitted signal in each slot is described by one or several resource grids of $N_{RB}^{UL} N_{SC}^{RB}$ subcarriers and N_{Symb}^{UL} OFDMA symbols. Fig. 5 illustrates the resource grid, where the uplink bandwidth $N_{RB}^{UL} = 50$, the subcarrier number in a resource block, $N_{SC}^{RB} = 12$, and the

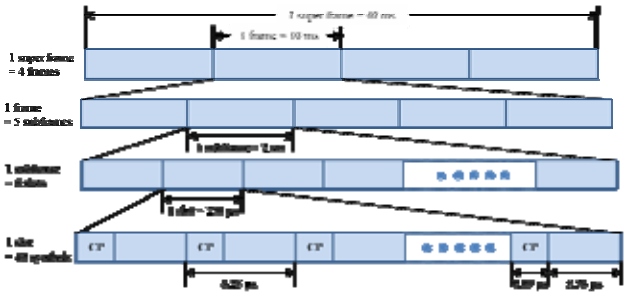

Fig. 4. Slot structure.

Table 2. OFDM Numerology.

Parameters	Values
System bandwidth (MHz)	**125**
Sampling rate (MHz)	184.32
Subcarrier spacing (kHz)	180
OFDM symbol length (FFT size)	1024
OFDM symbol duration (μs)	5.56
Cyclic prefix length (sample)	128
Cyclic prefix duration (μs)	0.69
Slot duration (μs)	250
Number of sample per slot	46080
Number of OFDM symbol per slot	40

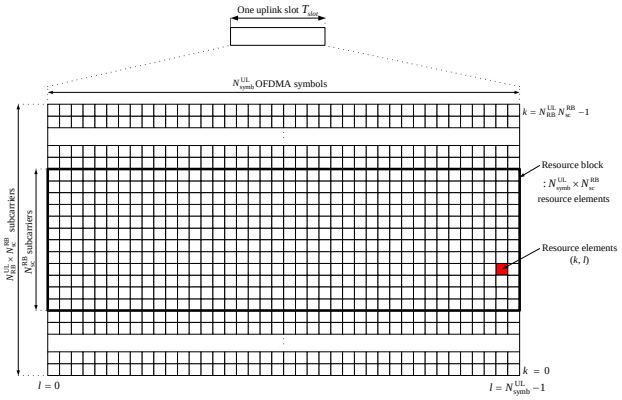

Fig. 5. Uplink resource grid.

number of OFDMA symbols in an uplink slot, $N_{Symb}^{UL} = 40$. Each element in the resource grid is called a resource element and is defined uniquely by the index pair (k, l) in a slot where $k = 0, 1, \cdots, N_{RB}^{UL} N_{SC}^{RB} - 1$ and $l = 0, 1, \cdots, N_{Symb}^{UL} - 1$ are the indices in the frequency and time domains, respectively. The resource element (k, l) is the smallest resource unit for uplink transmissions. A resource block is defined as N_{Symb}^{UL} consecutive OFDMA symbols in the time domain and N_{SC}^{RB} consecutive subcarriers in the frequency domain. Therefore, a resource block in the uplink consists of $N_{Symb}^{UL} N_{SC}^{RB}$ resource elements, corresponding to one slot in the time domain and 2.16

Fig. 6. Uplink data channel transmitter.

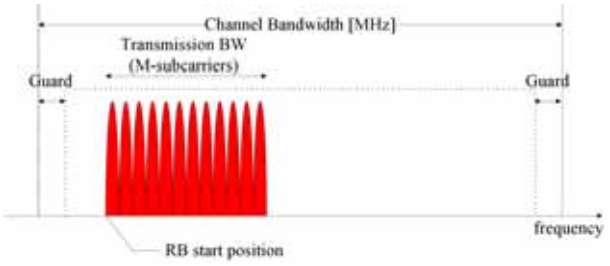

Fig. 7. Transmission spectrum of the uplink signal.

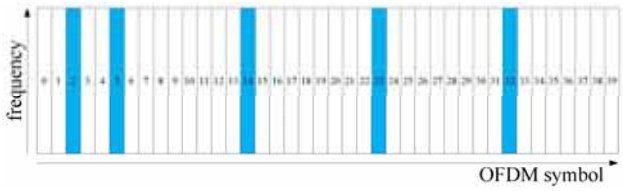

Fig. 8. Uplink data channel structure.

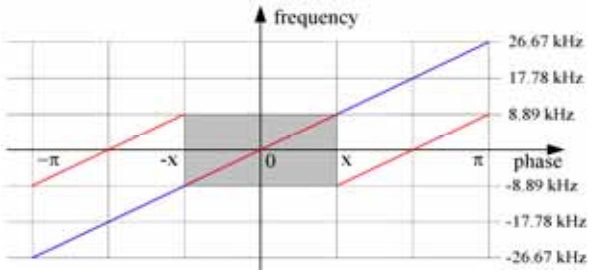

Fig. 9. Uplink frequency estimation range.

MHz in the frequency domain.

Fig. 6 presents the uplink data channel transmitter of the baseband modem for a mobile wireless backhaul. This is a kind of the OFDM modem that is used widely in cellular communications. On the other hand, it requires broadband high-speed signal processing because the system bandwidth is 125 MHz, and the sampling rate is 184.32 MHz. The system bandwidth can be also extended to 500 MHz (or 1 GHz if eight component carriers) by carrier aggregation. Therefore, the implementation of a millimeter-wave modem is difficult but important. The turbo code is used as an error correction code and the supported modulation schemes are QPSK, 16QAM and 64QAM. The resource element mapper maps the complex-valued modulation symbols into the resource elements of the resource blocks allocated for uplink transmission. Finally, the OFDM signal is generated through an IFFT operation. Fig. 7 presents the uplink transmission spectrum, as an example. The uplink signal occupies only the allocated bandwidth depending on the size of the assigned resource blocks. The uplink frequency is decided according to the start position of the resource blocks.

The uplink pilot symbols are inserted between the data symbols for the channel estimation at the receiver. In a HST moving at 400 km/h, the maximum Doppler shift is 20 kHz at 27 GHz when reflecting the uplink and downlink channel. To estimate the frequency offset, up to 20 kHz at the uplink receiver, the pilot symbol interval should be at least 4 symbols. This requires 10 pilot symbols, which is not effective in achieving high data throughput.

Fig. 8 shows the configuration of the uplink data channel in which the 'blue' colored symbols (#2, #5, #14, #23 and #32) mean the pilot symbol. The percentage of the pilot symbols is 12.5%. The pilot symbols are normally deployed at regular intervals. On the other hand, the designed uplink pilots aim to resolve the Doppler problem with fewer pilot symbols in a HST channel. Fig. 9 represents the frequency range that can be estimated by the pilot symbols in Fig. 7. The frequency offset f_1 (blue line) that can be estimated by pilots #2 and #5 is ±26.67 kHz. The frequency offset f_2 (red line) that can be estimated by pilots #5, #14, #23 and #32 is ±8.89 kHz. The final frequency offset f_o is calculated as follows:

$$f_o = \begin{cases} (f_1 + f_2)/2 & if\ |f_1| \le 8.89\,\text{kHz} \\ (f_1 + f_2)/2 + 8.89\text{kHz} & if\ f_1 > 8.89\,\text{kHz} \\ (f_1 + f_2)/2 - 8.89\text{kHz} & if\ f_1 < -8.89\,\text{kHz} \end{cases} \quad (1)$$

where offset f_1 value plays an important role as a reference to determine if the phase of f_2 is in the range (-x, x) or not.

3.3 Downlink

The downlink resource grid is same as the uplink. The transmitter of Fig. 5 is also used for the downlink, except that the downlink transmission spectrum occupies the entire system bandwidth. A multiplexing scheme in the downlink is OFDM due to the efficient use of the spectrum. In addition, it is less sensitive to timing offsets compared to other multiplexing schemes.

Because the millimeter-wave channel characteristics of small delay spread and large coherence bandwidth, cyclic prefix can be shortened and wide subcarrier spacing can be used to design a system robust to the Doppler Effect and frequency offset. Considering that the maximum velocity of mTE is 400 km/h causing a maximum Doppler shift of 10 kHz, the subcarrier spacing Δf of 180 kHz is suitable for the system. To reserve some subcarriers as guard bands, the total number of resource blocks of each component carrier is 50 and each resource block is defined as 40 consecutive OFDM symbols in the time domain and 12 consecutive subcarriers in the frequency domain, as illustrated in Fig. 10. The first four OFDM symbols are the resources for downlink control data transmission and others are for downlink data transmission.

Pilot signals, as shown in Fig. 10, play important roles

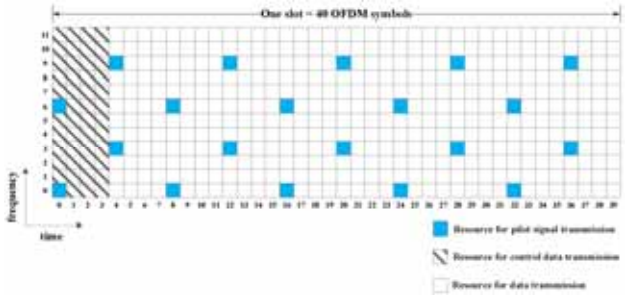

Fig. 10. Downlink channel structure.

in the system. In order to adapt to the rapidly changing channel of HSTs, accurate channel estimation by the pilot signals is highly important. Without accurate channel estimation information, the system performance will degrade significantly. In this paper, a least-squares (LS) channel estimation was used, and the estimated channel was interpolated using a FFT interpolation in the frequency domain and a linear interpolation in the time domain.

From the unique MHN structure with scarce reflectors and scatters and the effect of Tx/Rx beamforming, a line-of-sight (LOS) signal can be guaranteed in most cases, and the received power of the dominant path is much larger than that of the multipath signals. As a result, the Doppler spread, which is approximately equivalent to the Doppler shift in the frequency domain, can be overcame simply by automatic frequency control (AFC), whereas the Doppler spread in general cellular systems is difficult to compensate for. Therefore, the downlink uses a simple Doppler shift compensation algorithm similar to that described elsewhere [8]. The algorithm simply estimates the average Doppler frequency shift Δf_s using the received pilot signals and then directly compensates for it in the received signal $r(m)$. The received signal after the Doppler compensation, $\tilde{r}(m)$, can be expressed as follows,

$$\tilde{r}(m) = r(m) \cdot e^{-j2\pi\Delta f_s m T_s} \tag{2}$$

where T_s is the sampling interval. Owing to the short TTI of the system, the compensation period of the Doppler frequency offset will be shortened, leading performance enhancement.

4. Performance Evaluation

According to a previous report [9], studies of the propagation characteristics of 27.4 GHz have shown that the delay spread varies from 21.75 to 75.75 ns. Owing to this extremely small delay spread, the coherence bandwidth of the channel in this system is larger than 1 MHz. Even if Soma claims that the K-factor of the Rician fading channel, which refers to the ratio of the energy in the line-of-sight (LOS) path to the energy in the scattered paths, is smaller than 10 dB [9], the K-factor in the HST scenario would be much larger than that because of its unique environment that has scarce reflectors and scatters. Furthermore, this millimeter-wave system uses the fixed Tx/Rx beamforming at the mRUs of the mDU and mTE, which helps reduce the multipath signals. The antenna configuration is one transmit antenna and one receive antenna in the uplink and downlink. 3GPP, which examines the cellular communications, such as LTE/LTE-Advanced, modeled the HST environment in the open space scenario as the AWGN channel with a LOS path [10].

Table 3. Uplink Simulation Parameters.

Parameters	Values
Carrier frequency	**27 GHz**
Bandwidth (W)	125 MHz
Resource block	10 RBs
Modulation	QPSK, 16QAM, 64QAM
Channel code	Turbo code
Code rate (R_c)	0.8
Velocity (V)	400 km/h
Wireless channel	Rician (K=30,50,100)

The Rician probability density function (pdf) of a random variable x is

$$f(x) = \frac{x}{\sigma^2} e^{-\frac{(x^2+\upsilon^2)}{2\sigma^2}} I_0\left(\frac{x\upsilon}{\sigma^2}\right) \tag{3}$$

where $I_0(\cdot)$ is the modified Bessel function of the first kind with order zero, υ^2 is a LOS signal power, and $2\sigma^2$ is a non-LOS signal power. The Rician K-factor is defined as $K = \upsilon^2 / 2\sigma^2$. If the K-factor is zero, it becomes the Rayleigh fading channel. If the K-factor is ∞, it becomes the AWGN channel.

Therefore, link-level simulations have been conducted to evaluate the uplink and downlink performance under the Rician fading channel, respectively.

4.1 Uplink Channel

The uplink performances were evaluated under the single-path Rician channel with K-factors of 30, 50 and 100. Table 3 lists the uplink simulation parameters. The frequency offset estimation and compensation was applied in the uplink.

Fig. 11 shows the bit error rate (BER) performance of QPSK, 16QAM and 64QAM in the uplink. It is observed from Fig. 11 that they have good performance in the AWGN channel. On the other hand, only QPSK and 16QAM (K = 50, 100) are acceptable in the Rician channel. The BER performance can be improved further when the code rate is lower than 0.8 or the K-factor is large. Because the data of two uplink channels are different in a multi-flow communication, the total spectral efficiency is doubled. Therefore, the maximum spectral efficiencies are 2.09 bps/Hz for QPSK, 4.18 bps/Hz for 16QAM and 6.27

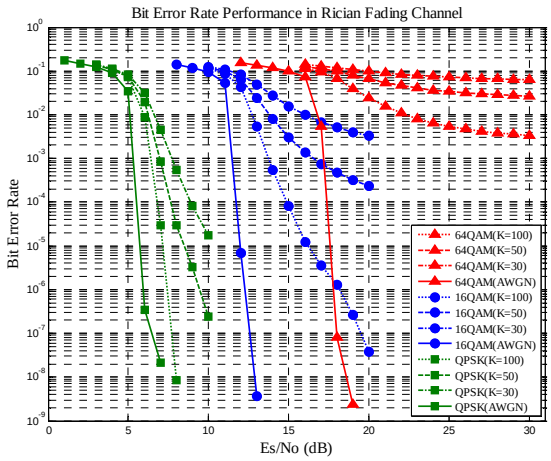

Fig. 11. BER performance of the uplink channel (V =400km/h, R_c =0.8).

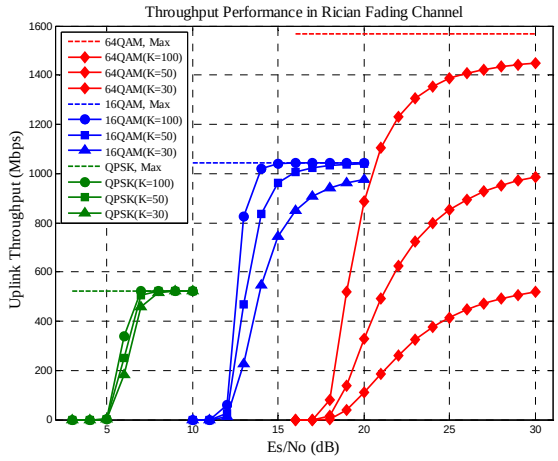

Fig. 12. Throughput performance of the uplink channel (V =400km/h, R_c =0.8, W =500MHz).

bps/Hz for 64QAM, respectively. The momentary spectral efficiency may reach the peak, when the Doppler shift variations are small. In addition, 64QAM is supported at a lower speed than 200 km/h.

If the UL/DL ratio is 50:50 in TDD and the system bandwidth is 500 MHz, as shown in Fig. 12, the maximum uplink data rates are 522.5 Mbps for QPSK, 1045 Mbps for 16QAM and 1567.5 Mbps for 64QAM, in a multi-flow communication. Therefore, it is possible to achieve a data rate more than 1 Gbps.

4.2 Downlink Channel

Similarly, the downlink performances were evaluated using the simulation parameters listed in Table 4.

Fig. 13 shows the BER versus SNR for the different K-factor and modulation schemes when the velocity of mTE is 400km/h. Performance degradation occurs when the K-factor becomes small. One reason for this is that the conventional AFC, which simply compensates for the Doppler frequency shift, cannot efficiently combat the Doppler spread, the effect of which destroys the

Table 4. Downlink Simulation Parameters.

Parameters	Values
Carrier frequency	**27 GHz**
Component carriers	**4**
Bandwidth (W)	500 MHz
Modulation	QPSK, 16QAM, 64QAM
Channel code	Turbo code
Code rate (R_c)	0.6, 0.8
Channel estimation	LS estimation
Delay spread	100 ns

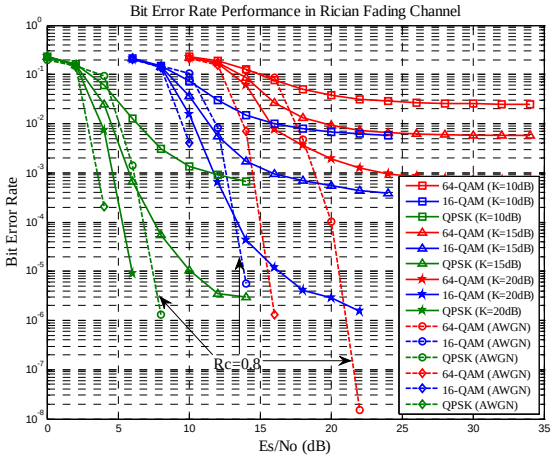

Fig. 13. BER performance of the downlink channel (V =400km/h, R_c =0.6).

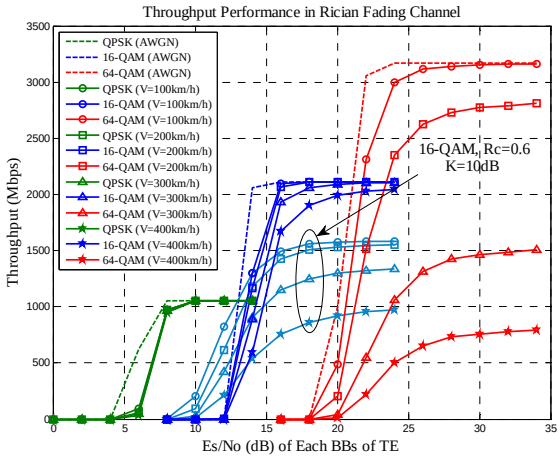

Fig. 14. Throughput performance of the downlink channel (K =20dB, R_c =0.8, W =500MHz).

orthogonality of the subcarriers, resulting in inter-carrier interference due to leakage among subcarriers.

Fig. 14 plots the downlink throughput for the different velocities of mTE and the different modulations. From the figure, it is better to use the modulation of QPSK in the low SNR region from 0 dB to 15 dB, and the throughput when using 16QAM can reach beyond 2 Gbps in the SNRs

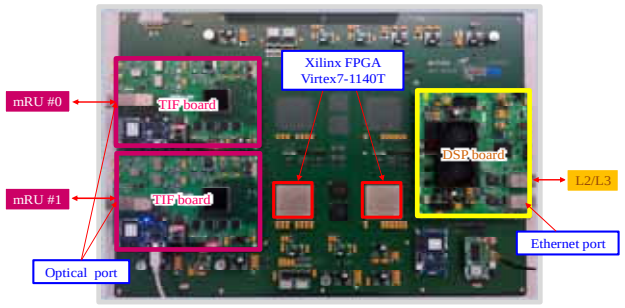

Fig. 15. Prototype of a mDU-BB board.

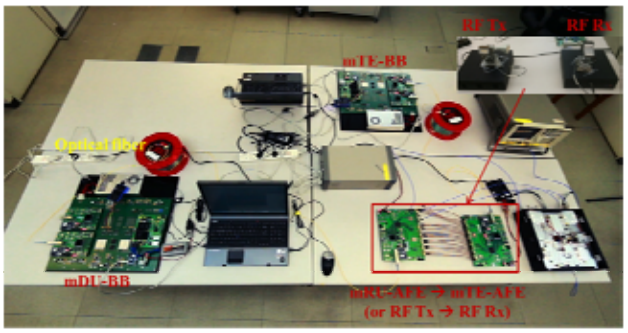

Fig. 16. Physical link test (mDU → mTE).

over 15 dB. Both QPSK and 16QAM were less sensitive to the velocity of mTE than 64QAM, which is highly vulnerable to the velocity. This means that for extremely high-speed moving trains, the velocity of which is over 300 km/h, 16QAM is the most appropriate modulation scheme in the system. To alleviate the degradation in performance of 64QAM, pilot signals in the time domain should be assigned more closely. More accurate channel estimation information is then provided to combat the short coherence time of the channel. The spectral efficiency can be calculated using the throughput simulation results obtained. The peak downlink spectral efficiency is approximately 4 bps/Hz in the case of 16QAM.

5. Implementation of the mmWave Modem

The millimeter-wave modem was implemented by Xilinx Virtex-7 FPGA products. Fig. 15 shows a prototype of mDU baseband (BB) board packaged with two FPGAs that function as a modem and a codec, respectively. A transceiver interface (TIF) board has an 10 Gbps optical transceiver that is interconnected with mRU via single mode optical fiber. The digital signal processor (DSP) (Texas Instruments, TMS320C6678) controls the physical layer operations and acts as an interface of the protocol stack (layer 2/3). The modem works in 184.32 MHz generated with a 10 MHz reference clock and the AD/DA conversions are performed in mRUs.

The physical link test was conducted in a laboratory to verify the functions of the implemented modem. Fig. 16

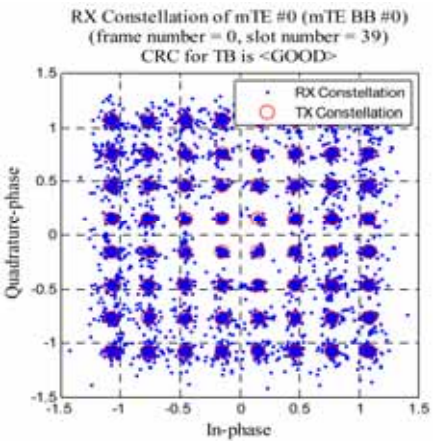

Fig. 17. Constellation under RF cable connection.

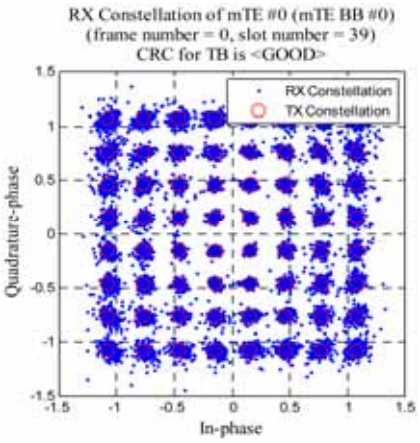

Fig. 18. Constellation under RF antenna connection.

shows a test configuration between the mDU and mTE in the downlink. The modulation signals of the mDU-BB are transmitted to the mRU-analog front end (AFE) (or RF Tx) through the optical fiber. Then the mRU-AFE (or RF Tx) and the mTE-AFE (or RF Rx) is connected with the RF cables or horn antennas. And the mTE-AFE (or RF Rx) signals are transmitted to the mTE-BB through the optical fiber. Finally, the mTE-BB demodulates the received downlink signal and checks the cyclic redundancy check (CRC) value of decoder output. When the demodulation is a success, a CRC value is 0. Fig. 17 illustrates the Tx/Rx constellations of 64QAM under the RF cable connection between the mRU-AFE and mTE-AFE. It was observed that a CRC value was 0 and an error vector magnitude (EVM) at the receiver was -24.71 dB. In addition, Fig. 18 shows the Tx/Rx constellations with the -22.4 dB EVM measured, when the 27 GHz horn antennas are used in the RF-Tx and RF-Rx. Although there is no mobility, this test result shows the possibility of applying the implemented mmWave modem to a mobile wireless backhaul.

6. Conclusion

This paper proposed the physical layer design of the

MHN uplink and downlink that uses millimeter-waves for a mobile wireless backhaul. The performance of the uplink and downlink were evaluated under the Rician fading channel conditions. The baseband prototype of a millimeter -wave communication modem was implemented by FPGA. The proposed MHN system can provide a high data rate service of Gbps in vehicles carrying hundreds of wireless Internet users. This study is expected to contribute to the research and development of millimeter-wave cellular communication systems.

Acknowledgement

This work was supported by the ICT R&D program of MSIP/IITP, Republic of Korea. [14-000-04-001, Development of 5G Mobile Communication Technologies for Hyper-connected Smart Services]

References

[1] O. B. Karimi, J. Liu, and C. Wang, "Seamless wireless connectivity for multimedia services in high speed trains," *IEEE Journal on Selected Areas In Comm.*, Vol. 30, No. 4, pp. 729-739, May 2012. Article (CrossRef Link)

[2] H. W. Chang, M. C. Tseng, S. Y. Chen, M. H. Cheng, and S. K. Wen, "Field trial results for integrated WiMAX and radio-over-fiber systems on high speed rail," in *Personal, Indoor and Mobile Radio Communications (PIMRC), 2011 IEEE 22nd International Symposium on*, Sept. 2011, pp. 2111-2115. Article (CrossRef Link)

[3] ITU-R M.1645, Framework and overall objectives of the future development of IMT-2000 and systems beyond IMT-2000, 2003. Article (CrossRef Link)

[4] 3GPP TR 36.913 v11.0.0, Requirements for further advancements for E-UTRA (LTE-Advanced) (Release 11), 2012-09. Article (CrossRef Link)

[5] RWS-120052, Report of 3GPP TSG RAN workshop on Release 12 and onwards, Ljubljana, Slovenia, June 2012. Article (CrossRef Link)

[6] J. Kim and I. Kim, "Distributed antenna system-based millimeter-wave mobile broadband communication system for high speed trains," International *Conf. on ICT Convergence*, October 2013. Article (CrossRef Link)

[7] S. Choi, D. You, I. Kim and D. Kim, "Uplink design of millimeter-wave mobile communication systems for high-speed trains," *IEEE 79th Vehicular Technology Conference*, May 2014.

[8] J. Li and Y. Zhao, "Radio environment map-based cognitive Doppler spread compensation algorithms for high-speed rail broadband mobile communications," *EURASIP Journal on Wireless Communications and Networking*, 2012. Article (CrossRef Link)

[9] P. Soma, L. C. Ong, S. Sun and M. Y. W. Chia, "Propagation measurements and modeling of LMDS radio channel in Singapore," *IEEE Trans. Veh. Technol.*, Vol. 52, no. 3, pp. 595-606, May 2003. Article (CrossRef Link)

[10] NTT DoCoMo, R4-070066, "Way forward on high speed train," www.3gpp.org, 3GPP TSG RAN WG4, meeting 42, St. Louis, US, February 2007. Article (CrossRef Link)

Seung Nam Choi received his B.S. and the M. S. degrees in electronic engineering from Chonnam National University, Gwangju, Korea, in 1998 and 2000, respectively. Since 2000, he has joined Electronics and Telecommunications Research Institute (ETRI), Korea, as a senior researcher. Currently, he is pursuing a Ph.D. degree in electronic engineering at Chonnam National University. His research interests include long term evolution (LTE), machine type communications (MTC), and millimeter-wave communications.

Junhyeong Kim received his B.S. degree in electronic engineering from Tsinghua University, Beijing, China, in 2008. He received his M.S. degree in electrical engineering from Korea Advanced Institute of Science and Technology (KAIST), Korea, in 2011. He is currently with Electronics and Telecommunications Research Institute (ETRI), Korea. His research interests include handover, cooperative communications, and MIMO technology for wireless communications.

Il Gyu Kim received his B.S. and the M.S. degrees in electronic engineering from The University of Seoul, Korea and his Ph.D. degree in information and communication engineering from Korea Advanced Institute of Science and Technology (KAIST), in 1995, 1997 and 2009, respectively. From 1997 to 1999, he was a senior searcher at Shinsegi Telecom. Since 1999, he has joined Electronics and Telecommunications Research Institute (ETRI), Korea, as a principal researcher. His research interests include WCDMA, LTE/LTE-Advanced, MIMO, and millimeter-wave communications.

Dae Jin Kim received his B.S. degree in electronic engineering from Seoul National University, Seoul, Korea, in 1984. His M. S. and the Ph.D. degrees in electrical engineering were conferred from the Korea Advanced Institute of Science and Technology (KAIST), Seoul, Korea, in 1986 and 1991, respectively. From 1991 to 1996, he worked for LG Electronics Inc., Seoul, Korea, developing HDTV and digital CATV transmitters and receivers. Since 1997 he has been a professor in the school of electronics and computer engineering at Chonnam National University, Gwangju, Korea. His recent research interests include the design and implementation of digital communication system and digital broadcasting system. He also has interests in smart TV and home networks.